CHAPTER

Generalized Flow and Heat Transfer in Porous Media

9

9.1 Introduction

Flow through porous media has been recognized as a fluid dynamics topic which has applications in a variety of engineering fields including seepage through soil, concrete, insulating media, and packed beds; flows in heat exchangers and alloy solidification; and cooling of electronic components. Several books on porous media flow and heat transfer have been published covering both analytical and numerical solution methodologies [1–4].

It appears that the usage of porous media flow models is divided into two parts. In the first of these we generally consider materials of low porosity (Fig. 9.1a) and relate *a priori* by physical law the quantity of flow passing through all the pores in the appropriate coordinate directions. Here we find that at low velocities, as generally occur here, the relationship is linear and the quantity of flow is related linearly to the pressure gradient. Thus, we generally write that (Darcy's law [5])

$$u_i = -\frac{\kappa}{\mu}\left(\frac{\partial p}{\partial x_i} - \rho g_i\right) \tag{9.1}$$

where u_i are the seepage velocity components, μ is the dynamic viscosity of the fluid, and κ is permeability of the medium expressed in m^2. The permeability may be directional and in such situations, κ will be a tensor [1]. We now concentrate on the balance of total quantities and consider a unit volume of porous medium to which we apply the mass conservation (incompressible flow) $\partial u_i/\partial x_i = 0$. Using directly the linear relationship [Eq. (9.1)] we immediately find that the following equation is obtained (ignoring the gravity effects):

$$\frac{\partial}{\partial x_i}\left(-\frac{\kappa}{\mu}\frac{\partial p}{\partial x_i}\right) = 0 \tag{9.2}$$

The problem now becomes simply a solution to a potential equation if either the pressure or its gradients are known at the boundaries and we have discussed such solutions using the finite element method in Ref. [1] and in Chapter 1 of this book. However, more recent and alternative application of porous media has been used at high porosities. We refer to this second category as a high-porosity model in which the porosity is large, often approaching unity. Such a model is extremely useful for some problems. For instance, a network of conduits distributed throughout the fluid

Finite Element Meth Fluid Dynam 7E, Volume 3. http://dx.doi.org/10.1016/B978-1-85617-635-4.00009-1

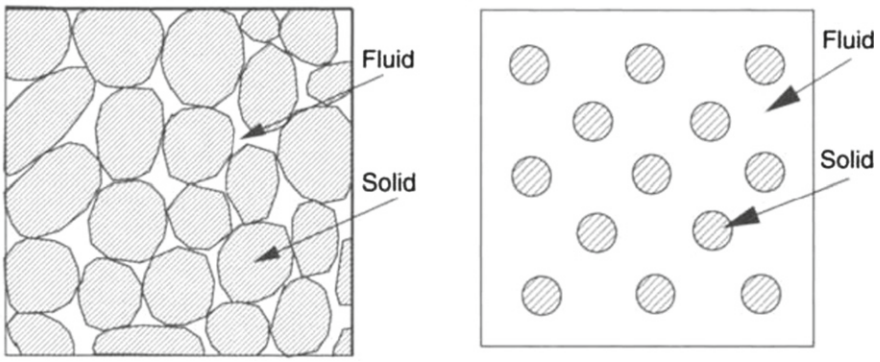

(a) Low porosity medium **(b)** High porosity medium

FIGURE 9.1
Typical examples of porous media.

and kept rigidly in space by external means is an example (Fig. 9.1b). This collection of obstructions will exact a force on the fluid in a complex manner. Now the relation between the force and the velocity is no longer linear as in the first model but can be determined by suitable experiments. Such models are generally useful for examples such as cooling of electronic components, flow past heat exchanger pipes, etc. At very high porosity we generally consider the equations to be almost those of Navier-Stokes to which an experimental addition of measured force values caused by the solid is carried out [6–10]. Various quadratic equations relating this force per unit volume to the velocity field and to the solid matrix geometry are available in the literature.

Clearly such models are generally valid if the volume of the obstructions is fairly small compared to the total volume [11,12] or if an interface is shared between a saturated porous medium and flow with no obstructions [13–15]. However, in prinicple this model can be used at low porosities but it will be very expensive. Thus, the low- and high-porosity models can be considered as two models dealing with different phenomena. A number of examples with the first type of model are included in Ref. [1] and we shall not consider this further again. However, we shall show how the problems can be dealt with using the generalized high-porosity models. In the following sections we derive the high-porosity model and present some examples.

9.2 A generalized porous medium flow approach

In this section, a generalized model for solving porous medium flows will be presented. Let us consider the balance of mass, momentum, and energy for two-dimensional flow in a fluid-saturated porous medium of variable porosity. We shall assume the medium to be isotropic with constant physical properties, except for the medium porosity. Let a^f be the fraction of area (nondimensional) available for flow per unit cross-sectional area (Fig. 9.2), at a location in a given direction. In fact, a^f is an averaged

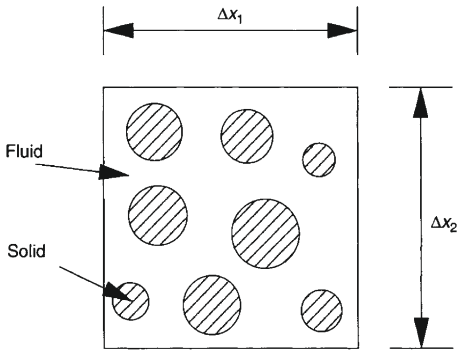

FIGURE 9.2
Fluid-saturated porous medium. Infinitesimal control volume.

quantity, the average being taken over the length scale of the voids (or the length scale of the particles, if the porous bed is made up of particles) in the flow direction. For an isotropic porous bed, a^f will be identical in all directions and can also be equal to the local bed porosity, ε. In spite of averaging over the void length scale, the fractional area a^f may vary from location to location on the macro-length scale "L" of the physical problem, due to the variation of the bed porosity.

The porosity, ε, of the medium is defined as

$$\varepsilon = \frac{\text{void volume}}{\text{total volume}} = \frac{a^f \Delta x_1 \Delta x_2}{\Delta x_1 \Delta x_2} = a^f \tag{9.3}$$

Now, the mass balance of an arbitrary control volume, as shown in Fig. 9.2, gives [9]

$$\frac{\partial \rho^f}{\partial t} + \frac{\partial (\rho^f {u_i}^f)}{\partial x_i} = 0 \tag{9.4}$$

where the superscript "f" stands for fluid, ρ is the density, and u_i are the velocity components in the x_i directions, respectively. The volume-averaged velocity components may be defined as [4]

$$u_i = \varepsilon {u_i}^f \tag{9.5}$$

Equation (9.4) can be simplified for an incompressible flow (constant density) as follows:

$$\frac{\partial u_i}{\partial x_i} = 0 \tag{9.6}$$

Similarly, the equation for momentum balance can be derived as

$$\frac{\rho^f}{\varepsilon}\left[\frac{\partial u_i}{\partial t}+\frac{\partial}{\partial x_j}\left(\frac{u_i u_j}{\varepsilon}\right)\right]=-\frac{1}{\varepsilon}\frac{\partial}{\partial x_i}(p^f\varepsilon)+\frac{\mu_e}{\varepsilon}\frac{\partial^2 u_i}{\partial x_i^2}-D_{x_i}+\rho^f g_i \tag{9.7}$$

where μ_e is the equivalent viscosity, p^f is the fluid pressure; g_i is the acceleration due to gravity, and D_{x_i} is the matrix drag per unit volume of the porous medium. Equation (9.7) may be written in conservation form as (not essential for solving incompressible flow problems)

$$\frac{1}{\varepsilon}\left[\frac{\partial U_i}{\partial t}+\frac{\partial}{\partial x_j}\left(\frac{U_i u_j}{\varepsilon}\right)\right]=-\frac{1}{\varepsilon}\frac{\partial}{\partial x_i}(p^f\varepsilon)+\frac{1}{\varepsilon}\frac{\partial \tau_{ij}}{\partial x_j}-D_{x_i}+\rho^f g_i \tag{9.8}$$

where $U_i=\rho^f u_i$ and

$$\tau_{ij}=\mu_e\left(\frac{\partial u_i}{\partial x_j}+\frac{\partial u_j}{\partial x_i}\right) \tag{9.9}$$

Several experimental correlations are available for the matrix drag, D_{x_i}, and one of them is the experimental data reported by Ergun [16]. The Ergun correlation is written as

$$D_{x_i}=\frac{\mu^f u_i}{\kappa}+\frac{1.75}{\sqrt{150}}\frac{\rho^f}{\sqrt{\kappa}}\frac{|\mathbf{u}|}{\varepsilon^{3/2}}u_i \tag{9.10}$$

where $\mathbf{u}$ is the velocity vector in the field. The final form of the governing equations for incompressible flow through a porous medium in dimensional form may be written as

Continuity

$$\frac{\partial u_i}{\partial x_i}=0 \tag{9.11}$$

Momentum

$$\frac{\rho^f}{\varepsilon}\left[\frac{\partial u_i}{\partial t}+\frac{\partial}{\partial x_j}\left(\frac{u_i u_j}{\varepsilon}\right)\right]=-\frac{1}{\varepsilon}\frac{\partial}{\partial x_i}(p^f\varepsilon)+\frac{\mu_e}{\varepsilon}\frac{\partial^2 u_i}{\partial x_i^2}-\frac{\mu^f u_i}{\kappa}-\frac{1.75}{\sqrt{150}}\frac{\rho^f}{\sqrt{\kappa}}\frac{|\mathbf{u}|}{\varepsilon^{3/2}}u_i+\rho^f g_i \tag{9.12}$$

If the porosity of the medium is small ($\varepsilon \to 0$) the velocity values will be small and the nonlinear term in Eq. (9.12) will also be small compared to the linear drag term. Thus, if the porosity approaches zero, the linear drag term (Darcy term) becomes prominent and all other terms will be negligibly small, leading to an approximation of Eq. (9.1). the other hand if the porosity approaches unity ($\varepsilon \to 1$), the incompressible fluid equations are recovered. It is therefore possible to solve problems in which both single phase fluid and porous medium are part of the same domain [13]. Thus applications such as alloy solidification, which involves solid, liquid, and porous mushy regions, can be tackled easily using the proposed approach [17]. The energy conservation equation is also derived in a similar manner. The final form of the energy equation is

Energy

$$\left[\varepsilon(\rho c_p)^f + (1-\varepsilon)(\rho c_p)^s\right]\frac{\partial T}{\partial t} + (\rho c_p)^f u_i \frac{\partial T}{\partial x_i} = k\left(\frac{\partial^2 T}{\partial x_i^2}\right) \tag{9.13}$$

In the above equation, c_p is the specific heat, T is the temperature, and k is the equivalent thermal conductivity. The superscripts f and s stand for the fluid and solid phases, respectively.

It should be noted that the permeability and thermal conductivity values can be directional, in which case they are tensors.

9.2.1 Nondimensional scales

The following final form of the nondimensional equations may be obtained by suitable scaling. The nondimensional scales used here are taken based on the assumption that the energy and momentum equations are weakly coupled via local density variation (see Chapter 6).

Continuity equation

$$\frac{\partial u_i^*}{\partial x_i^*} = 0 \tag{9.14}$$

Momentum equations

$$\begin{aligned}\frac{1}{\varepsilon}\frac{\partial u_i^*}{\partial t^*} + \frac{1}{\varepsilon}u_j^*\frac{\partial}{\partial x_j^*}\left(\frac{u_i^*}{\varepsilon}\right) &= -\frac{1}{\varepsilon}\frac{\partial}{\partial x_i^*}(\varepsilon p_f^*) - \frac{u_i^*}{ReDa} \\ &- \frac{1.75}{\sqrt{150}}\frac{|\mathbf{u}^*|}{\sqrt{Da}}\frac{u_i^*}{\varepsilon^{3/2}} + \frac{J}{Re\varepsilon}\left(\frac{\partial^2 u_i^*}{\partial x_i^{*2}}\right) + \gamma_i\frac{Gr}{Re^2}T^*\end{aligned} \tag{9.15}$$

Energy equation

$$\sigma\frac{\partial T^*}{\partial t^*} + u_i^*\frac{\partial T^*}{\partial x_i^*} = \frac{k^*}{RePr}\left(\frac{\partial^2 T^*}{\partial x_i^{*2}}\right) \tag{9.16}$$

In the above equations, the parameters governing the flow and heat transfer are the Darcy number (Da), Reynolds number (Re), Prandtl number (Pr), Grashoff number (Gr), ratio of heat capacities (σ), porosity of the medium (ε), conductivity ratio (k^*), and viscosity ratio (J), and γ_i is the unit vector in the buoyancy direction. The definitions for the scales and nondimensional parameters are

$$\begin{gathered}x_i^* = \frac{x_i}{L},\quad u_i^* = \frac{u_i}{u_a},\quad t^* = \frac{tu_a}{L},\quad p_f^* = \frac{p_f}{\rho_f {u_a}^2},\quad T^* = \frac{T-T_a}{T_w-T_a},\quad J = \frac{\mu_e}{\mu_f} \\ \sigma = \frac{\varepsilon(\rho c_p)_f + (1-\varepsilon)(\rho c_p)_s}{(\rho c_p)_f},\quad k^* = \frac{k}{k_f},\quad Re = \frac{\rho_f u_a L}{\mu_f} \\ Pr = \frac{\nu_f}{\alpha_f},\quad Da = \frac{\kappa}{L^2},\quad Gr = \frac{g\beta\Delta T L^3}{\nu_f^2}\end{gathered} \tag{9.17}$$

where subscripts a and f respectively refer to a free stream quantity and fluid and the subscript w indicates a wall. The above scales are suitable for most forced and mixed convection problems. However, for buoyancy driven flows, it is convenient to handle the equations using the following definition of the Rayleigh number (Ra), i.e.,

$$Ra = \frac{g\beta\Delta T L^3}{\nu\alpha} \tag{9.18}$$

where the following different scales need to be employed in solving natural convection problems:

$$u_i^* = \frac{u_i L}{\alpha_f}, \quad t^* = \frac{t\alpha_f}{L^2}, \quad p^* = \frac{pL^2}{\rho_f \alpha_f^2} \tag{9.19}$$

The nondimensional governing equations for natural convection are

Continuity equation

$$\frac{\partial u_i^*}{\partial x_i^*} = 0 \tag{9.20}$$

Momentum equations

$$\frac{1}{\varepsilon}\frac{\partial u_i^*}{\partial t^*} + \frac{1}{\varepsilon}u_j^*\frac{\partial}{\partial x_j^*}\left(\frac{u_i^*}{\varepsilon}\right) = -\frac{1}{\varepsilon}\frac{\partial}{\partial x_i^*}(\varepsilon p_f^*) - \frac{Pru_i^*}{Da}$$
$$-\frac{1.75}{\sqrt{150}}\frac{|\mathbf{u}^*|}{\sqrt{Da}}\frac{u_i^*}{\varepsilon^{3/2}} + \frac{JPr}{\varepsilon}\left(\frac{\partial^2 u_i^*}{\partial x_i^{*2}}\right) + \gamma_i Ra Pr T^* \tag{9.21}$$

Energy equation

$$\sigma\frac{\partial T^*}{\partial t^*} + u_i^*\frac{\partial T^*}{\partial x_i^*} = k^*\left(\frac{\partial^2 T^*}{\partial x_i^{*2}}\right) \tag{9.22}$$

Other alternative scales are possible and the appropriate references should be consulted to learn more about scaling. In the above formulation, the buoyancy effects are incorporated by invoking the Boussinesq approximation as discussed in Chapter 6. The kinematic viscosity ν, used in the above scales, is defined as

$$\nu = \frac{\mu}{\rho} \tag{9.23}$$

and α is the thermal diffusivity, given as

$$\alpha_f = \frac{k_f}{(\rho c_p)_f} \tag{9.24}$$

It may be observed that the scales and nondimensional parameters are defined by using the fluid properties. Often, a quantity called the Darcy-Rayleigh number is used in the literature as a governing nondimensional parameter for Darcy flow. This is the product of the Darcy (Da) and fluid Rayleigh (Ra) numbers defined previously. For isothermal flow problems, the energy equation is not solved.

9.3 Discretization procedure

The CBS scheme will be employed to solve the porous medium flow equations. In this context the same four steps, with minor modifications, will be utilized as discussed in Chapter 3.

The momentum equation is subjected to the CBS procedure and finite element discretization, as discussed in Chapter 3. Following Eq. (3.51), we may write the first step of the CBS algorithm for porous medium equations as (assuming constant ε)

$$\frac{\rho^f}{\varepsilon}\Delta\tilde{\mathbf{u}}^\star = -\mathbf{M}_u^{-1}\Delta t\left[\left(\frac{\rho^f}{\varepsilon^2}\mathbf{C}_u\tilde{\mathbf{u}}^n + \frac{1}{\varepsilon}\mathbf{K}_\tau\tilde{\mathbf{u}}^{n+\theta_3} + \mathbf{M}_d\tilde{\mathbf{u}}^{n+\theta_4} - \mathbf{f}^n\right)\right.$$
$$\left. - \Delta t\left(\frac{\rho^f}{\varepsilon^2}\mathbf{K}_u\tilde{\mathbf{u}} + \mathbf{C}_s\tilde{\mathbf{u}} + \mathbf{f}_s\right)^n\right] \tag{9.25}$$

All the matrices except $\mathbf{M}_d$ and $\mathbf{C}_s$ are defined and described in Chapter 3. The undefined matrices are

$$\mathbf{M}_d = D_p\mathbf{M}_u \quad \text{and} \quad \mathbf{C}_s = -\tfrac{1}{2}\int_\Omega [\nabla^{\mathrm{T}}(\mathbf{u}\mathbf{N}_u)]^{\mathrm{T}} D_p(\mathbf{u}\mathbf{N}_u)\mathrm{d}\Omega \tag{9.26}$$

where

$$D_p = \left[\frac{\mu^f}{\kappa} + \frac{1.75}{\sqrt{150}}\frac{\rho^f}{\sqrt{\kappa}}\frac{|\mathbf{u}|^n}{\varepsilon^{3/2}}\right] \tag{9.27}$$

For a smooth solution, the parameter θ_4 should be nonzero and equal to or below unity. $\theta_3 = 0$ gives a semi-implicit scheme and $\theta_3 = 1$ gives a quasi-implicit scheme. The superscript θ should be interpreted as

$$f^{n+\theta} = \theta f^{n+1} + (1-\theta) f^n \tag{9.28}$$

where the superscript n indicates the nth time iteration. Following the CBS algorithm in Chapter 3, semi- and quasi-implicit forms of the method are discussed in the next subsection.

9.3.1 Semi- and quasi-implicit forms

Single phase incompressible fluid flow problems can be solved in a fully explicit form, which is quite popular in fluid dynamics calculations [18]. However, a solution to the generalized porous medium equations using a fully explicit form has been less successful although some recent attempts have been made [19]. This is mainly due to the large values of the solid matrix drag terms, especially at smaller Darcy numbers. In order to eliminate some of the time step restrictions imposed by these terms, schemes other than the fully explicit forms are discussed below.

In the semi-implicit (SI) form [20], the porous medium source terms are treated implicitly. In other words, $\theta_1 = \theta_2 = \theta_4 = 1$ [see Eqs. (3.56) and (9.25)] and $\theta_3 = 0$, i.e.,

$$\tilde{\mathbf{u}}^{\star} = \left[\frac{\rho^f}{\varepsilon} + \Delta t D_p\right]^{-1} \left\{\frac{\rho^f}{\varepsilon}\mathbf{u}^n - \mathbf{M}_u^{-1}\Delta t \left[\left(\frac{\rho}{\varepsilon^2}\mathbf{C}_u\tilde{\mathbf{u}}^n + \frac{1}{\varepsilon}\mathbf{K}_\tau\tilde{\mathbf{u}}^n - \mathbf{f}^n\right) - \Delta t\left(\frac{\rho^f}{\varepsilon^2}\mathbf{K}_u\tilde{\mathbf{u}} + \mathbf{C}_s\tilde{\mathbf{u}} + \mathbf{f}_s\right)^n\right]\right\} \tag{9.29}$$

The Step 2 pressure calculation becomes [see Eq. (3.56)]

$$\Delta t\mathbf{H}\tilde{\mathbf{p}}^{n+1} = \left[\frac{\rho^f}{\varepsilon} + \Delta t D_p\right]\mathbf{G}\tilde{\mathbf{u}}^{\star} \tag{9.30}$$

Step 3 is given as

$$\Delta\tilde{\mathbf{u}}^{**} = \Delta\tilde{\mathbf{u}} - \Delta\tilde{\mathbf{u}}^{*} = -\Delta t\left[\frac{\rho^f}{\varepsilon} + \Delta t D_p\right]^{-1}\mathbf{G}\tilde{\mathbf{p}}^{n+1} \tag{9.31}$$

As seen the semi-implicit form described at Step 1 avoids simultaneous solution of the algebraic equations [20]. A suitable Poisson equation solver is required at Step 2. The quasi-implicit (QI) [21] form is very similar to that of the above scheme but now the viscous, second-order terms are also treated implicitly ($\theta_3 = 1$) [9]. The important difference, however, is that the quasi-implicit scheme does not benefit from mass lumping when solving for the intermediate velocity values. A simultaneous solution of the LHS matrices is essential here. It has been proven that both the QI and SI schemes generally perform well as shown elsewhere [22].

For nonisothermal flows, Eq. (9.13) is also solved along with the three steps of isothermal flows discussed above. To solve this convection-diffusion equation, any of the methods discussed in Chapter 2 may be employed. For forced convective heat transfer problems, the flow field may be established first before solving for the temperature field. However, in buoyancy driven flows a weak, simultaneous coupling between temperature and flow field exists and thus the flow and temperature equations should be solved simultaneously.

9.4 Forced convection

Flow through packed beds is important in many chemical engineering applications. Generally, the grain size in the packed beds will vary depending on the application. As the particle size increases, the packing close to the walls will become nonuniform thereby creating a channelling effect close to the solid walls. In such cases, the porosity value can be close to unity near the walls but will decrease to a free stream value away from the walls.

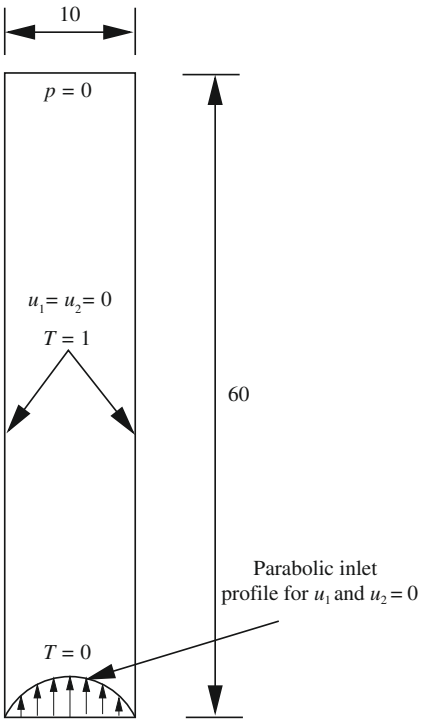

FIGURE 9.3
Forced convection in a channel filled with a variable porosity medium. Geometry and boundary conditions.

In such situations, the ability to vary the porosity within the domain itself is essential in order to obtain a correct solution. Although the theoretical determination of the near-wall porosity variation is difficult, there are some experimental correlations available to tackle this issue. One such widely employed correlation, given by Berenati and Brosilow [23], will be used here, i.e.,

$$\varepsilon = \varepsilon_e \left[1 + \exp\left(-\frac{cl}{d_p}\right)\right] \tag{9.32}$$

where ε_e is the free stream bed porosity taken to be equal to 0.39, c is an empirical constant ($c = 2$ for $d_p = 5$ mm), and l is the shortest distance to the wall. In general, the problem in this case is formulated based on the particle size d_p, i.e., the Reynolds number is based on the particle size.

Example 9.1. Forced convection heat transfer in a packed channel

Figure 9.3 shows the problem definition of forced flow through a packed bed. The inlet channel width is 10 times the size of the grain. The length of the channel is 10 times that of the inlet width. Zero pressure conditions are assumed at the exit.

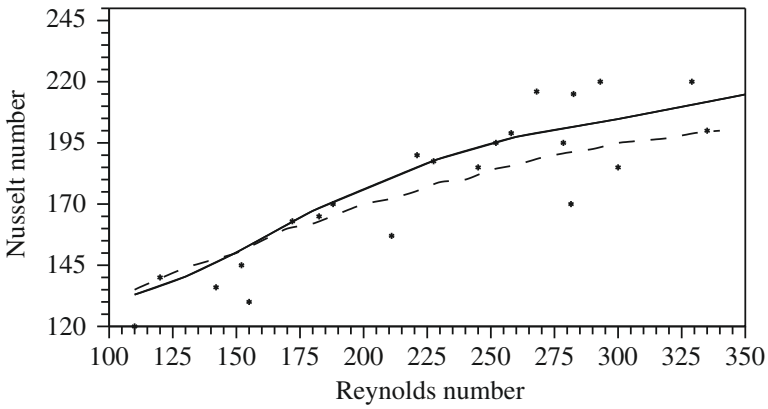

FIGURE 9.4

Forced convection in a channel. Comparison of Nusselt number with experimental data for different particle Reynolds numbers. Points—experimental [24]; dashed line—numerical [24]; solid line—CBS.

The inlet velocity profile is parabolic and no-slip boundary conditions apply on the solid side walls. Both the walls are assumed to be at a higher, uniform temperature than the inlet fluid temperature. The analysis is carried out for different particle Reynolds numbers ranging from 150 to 350. The *quasi-implicit* (QI) scheme with $\theta_3 = \theta_4 = 1$ has been employed to solve this problem. A nonuniform mesh with triangular elements was also used in the analysis. The mesh is fine close to the walls and coarse toward the center. The total number of nodes and elements used in the calculation is 3003 and 5776, respectively.

Figure 9.4 shows a comparison of the calculated steady-state average Nusselt number distribution on a hot wall with the available experimental and numerical data. The Nusselt number is calculated as

$$Nu = \frac{hL}{k} = \int_0^L \frac{\partial T}{\partial x_1} dl \tag{9.33}$$

Figure 9.5 shows the difference between the generalized model and the Brinkman [25] and Forcheimmer [26] extensions for the velocity profiles close to the wall in a variable porosity medium at steady state. As may be seen the Forcheimmer and Brinkman extensions fail to predict the channelling effect close to the wall. While the Brinkman extension is insensitive to porosity values, the Forcheimmer model does not predict the viscous effect close to the channel walls.

9.5 Natural convection

The fluid flow in a variable porosity medium within an enclosed cavity under the influence of buoyancy is another interesting and difficult problem to analyze. In order

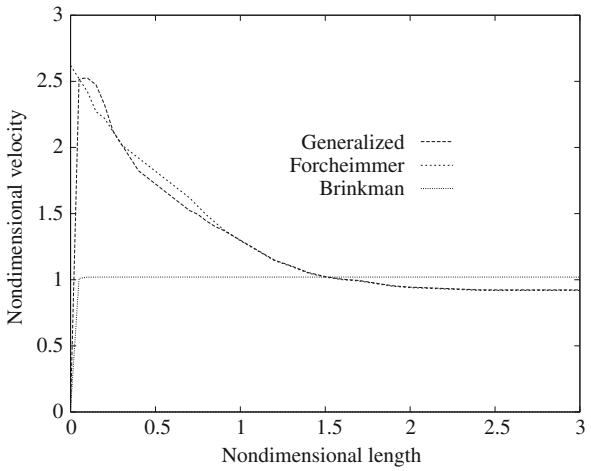

FIGURE 9.5

Forced convection in a channel. Comparison between the generalized model and the Forcheimmer and Brinkman extensions to Darcy's law.

to study such a problem, an enclosure packed with a fluid-saturated porous medium is considered as in the following example.

Example 9.2. Buoyancy driven convection in a packed enclosure

The aspect ratio of the enclosure is 10 (ratio between height and width). All the enclosure walls are subjected to "no-slip" boundary conditions. The left vertical wall is assumed to be at a higher, uniform temperature than the right side wall. Both the horizontal walls are assumed to be insulated (Fig. 9.6). The properties of the saturating fluid are assumed to be constant other than that of the density. The density variation is invoked by the Boussinesq approximation.

Table 9.1 shows the steady-state quantitative results and a comparison with the available numerical and experimental data. These data were obtained on a nonuniform structured 61x61 mesh. The accuracy of the prediction can be improved by further refinement of the mesh. An extremely fine mesh is essential near the cavity walls in order to predict the channelling effect in this region. In Table 9.1, experimental data is obtained from Ref. [27] and the numerical data for comparison is obtained from Ref. [28]. The following Nusselt number relation was used for this problem:

$$Nu = \frac{1}{L}\int_0^L \frac{\partial T}{\partial x} dl \tag{9.34}$$

9.5.1 Constant-porosity medium

Problems where the variation in porosity is of less significance normally occur in porous media that have small solid particle sizes. For instance, thermal insulation is one such example where the variation in porosity near the solid walls is not important

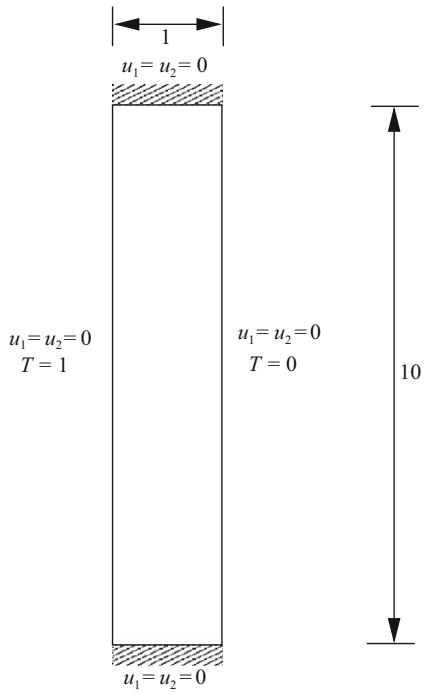

FIGURE 9.6
Natural convection in a fluid-saturated variable-porosity medium. Problem boundary conditions.

Table 9.1 Average Hot Wall Nusselt Number Distribution for Natural Convection in a Variable Porosity Medium, Aspect Ratio = 10

Fluid	d_p	ε_e	Pr	k^*	Ra	Experimental	Numerical	CBS
Water	5.7	0.39	7.1	1.929	1.830×10^7	2.595	2.405	2.684
					3.519×10^7	3.707	3.496	3.892
Ethyl alcohol	5.7	0.39	2.335	15.4	2.270×10^8	12.56	13.08	12.17
					3.121×10^8	15.13	15.57	14.28

but the uniform free stream porosity value can be very high. In order to investigate such media, a benchmark problem involving buoyancy driven convection in a square cavity has been solved.

Example 9.3. Buoyancy driven flow in a cavity filled with fluid-saturated constant-porosity medium

The problem definition is similar to the one shown in Fig. 9.6, the difference being that the aspect ratio is unity. The square enclosure is filled with a fluid-saturated

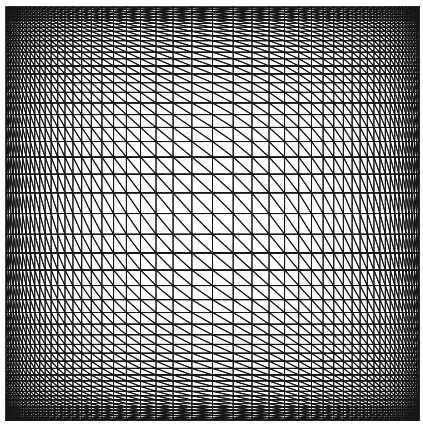

FIGURE 9.7
Buoyancy driven flow in a fluid-saturated porous medium. Finite element mesh (nodes: 2601, elements: 5000).

porous medium with constant and uniform properties except for the density, which is again incorporated via the Boussinessq approximation. A 51×51 nonuniform mesh (Fig. 9.7) is employed for this problem.

In Fig. 9.8, we show the velocity and temperature distribution at different Darcy and Rayleigh numbers. In this case the product of the Darcy and Rayleigh numbers is kept at a constant value in order to amplify the non-Darcy effects. It is clearly obvious that the maximum velocity in the Darcy flow regime, at a Darcy number of 10^{-6}, is located very close to the solid walls. The non-Darcy velocity profile, at a Darcy number of 10^{-2}, on the other hand looks very similar to that of a single phase fluid and the maximum velocity is located away from the solid walls. At a Darcy number of 10^{-4} the flow undergoes a transition from a Darcy flow regime to a non-Darcy flow regime. The temperature contours also undergo noticeable changes as the Darcy number increases from 10^{-6} to 10^{-2}.

Both the scheme and the model implementation have been designed in such a way that as the Darcy number increases, the flow approaches a single phase fluid flow, which is evident from Fig. 9.8.

In Table 9.2, the quantitative results obtained from the above analysis (only for the Darcy flow regime, $Da < 10^{-5}$) are compared with other available analytical and numerical results. In Table 9.2, the analytical solution has been obtained from Refs. [29], and "Numerical 1" and "Numerical 2" have been obtained from Refs. [30,31] respectively.

Example 9.4. Buoyancy driven convection in an axisymmetric enclosure filled with fluid-saturated constant-porosity medium

In order to compare the present numerical results with experimental data, an axisymmetric model was developed and a buoyancy driven flow problem was studied. The boundary and initial conditions are the same as for the previous problem,

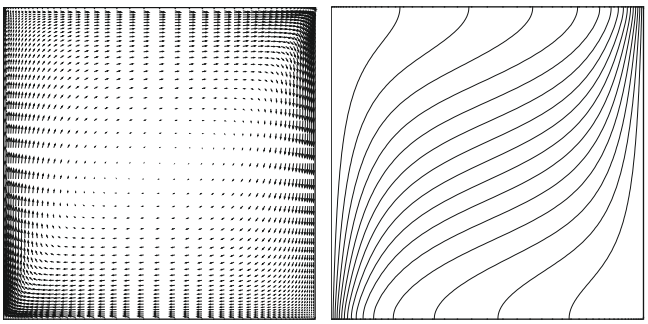

(a) Vector plot **(b)** Temperature

$Ra = 10^8,\ Da = 10^{-6}$

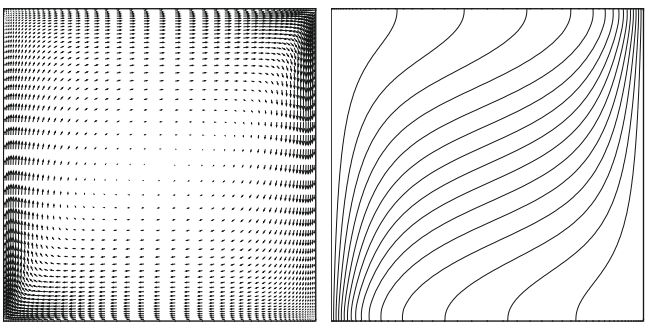

(c) Vector plot **(d)** Temperature

$Ra = 10^6,\ Da = 10^{-4}$

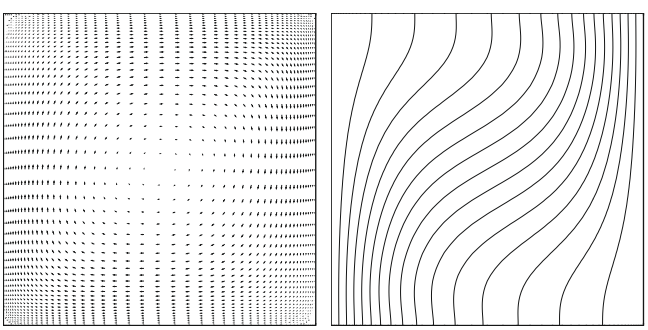

(e) Vector plot **(f)** Temperature

$Ra = 10^4,\ Da = 10^{-2}$

FIGURE 9.8

Natural convection in a fluid-saturated porous, square enclosure. Vector plots and temperature contours for different Rayleigh and Darcy numbers, $Pr = 0.71$.

Table 9.2 Average Nusselt Number Comparison with Analytical and Numerical Results

	Nu			
Ra* = RaDa	**Analytical**	**Numerical 1**	**Numerical 2**	**CBS**
10	–	1.07	–	1.08
50	1.98	–	2.02	1.96
100	3.09	3.09	3.27	3.02
500	8.40	–	–	8.38
1000	12.49	13.41	18.38	12.52

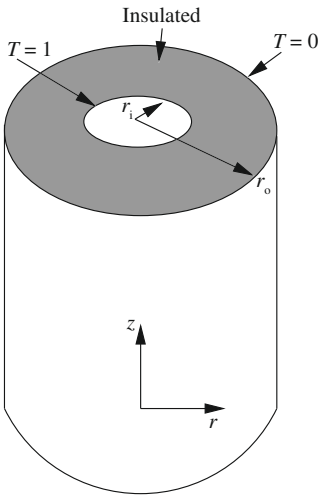

FIGURE 9.9
Natural convection in a fluid-saturated constant-porosity medium. Problem definition.

the main difference being in the definition of the geometry. In this case, the geometry is an annulus with a radius ratio (ratio between outer and inner radii) of 5.338 (see Fig. 9.9). The fluid used to saturate the medium is water with a Prandtl number of 5. The results are generated for different Grashof numbers (Ra/Pr) and compared with the experimental Nusselt number predictions as shown in Fig. 9.10. In general the agreement is excellent for the range of Grashof numbers considered.

9.6 Concluding remarks

In this chapter a brief summary of flow through porous media has been discussed. It is important to fully understand the concepts given in Chapter 3 before carrying out the porous medium flow calculations. The brief overview given in this chapter

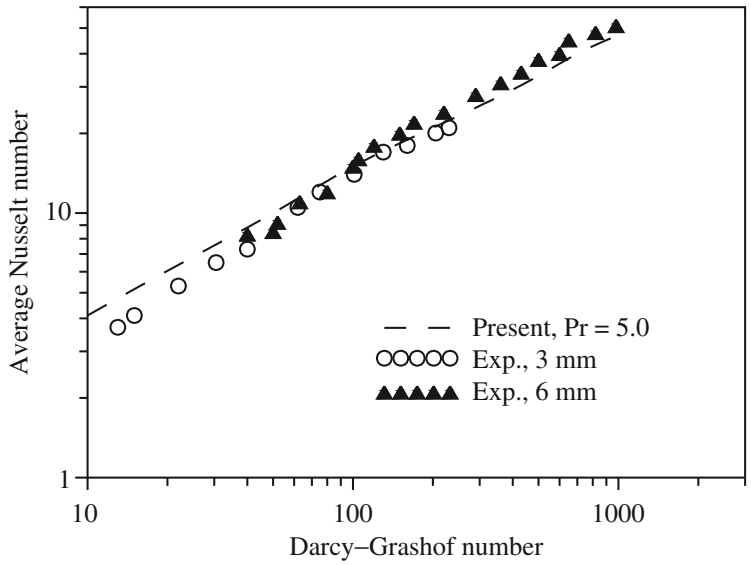

FIGURE 9.10

Natural convection in a fluid-saturated constant-porosity medium within an annular enclosure. Comparison of hot wall steady-state Nusselt number with the experimental and numerical data [32].

provides the reader with essential knowledge on how the CBS scheme is extended to a nonstandard fluid dynamics problem.

References

[1] O.C. Zienkiewicz, A.H.C. Chan, M. Pastor, B.A. Schrefler, T. Shiomi, Computational Geomechanics with Special Reference to Earthquake Engineering, John Wiley & Sons, Chichester, 1999.

[2] R.W. Lewis, B.A. Schrefler, The Finite Element Method in the Deformation and Consolidation of Porous Media, John Wiley & Sons, Chichester, 1998.

[3] M. Kaviany, Principles of Heat Transfer in Porous Media, Springer-Verlag, New York, 1991.

[4] D.A. Nield, A. Bejan, Convection in Porous Media, Springer Verlag, New York, 1992.

[5] H. Darcy, in: Victor Dalmont (Ed.), Les fontaines publiques de la ville de Dijon, Paris, 1856.

[6] S. Whitaker, Diffusion and dispersion in porous media, Am. Inst. Chem. Eng. J. 13 (1961) 420–427.

[7] K. Vafai, C.L. Tien, Boundary and inertia effects on flow and heat transfer in porous media, Int. J. Heat Mass Transfer 24 (1981) 195–203.

[8] C.T. Hsu, P. Cheng, Thermal dispersion in a porous medium, Int. J. Heat Mass Transfer 33 (1990) 1587–1597.
[9] P. Nithiarasu, K.N. Seetharamu, T. Sundararajan, Natural convective heat transfer in an enclosure filled with fluid saturated variable porosity medium, Int. J. Heat Mass Transfer 40 (1997) 3955–3967.
[10] P. Nithiarasu, K.N. Seetharamu, T. Sundararajan, Finite element modelling of flow, heat and mass transfer in fluid saturated porous media, Arch. Comput. Methods Eng., State of the Art Reviews 9 (2002) 3–42.
[11] K.I. Salas, A.M. Waas, Convective heat transfer in open cell metal foams, J. Heat Transfer-Trans. ASME 129 (9) (2007) 1217–1229.
[12] G. Laschet, Forchheimer law derived by homogenization of gas flow in turbomachines, J. Comput. Appl. Math. 215 (2) (2008) 467–476.
[13] N. Massarotti, P. Nithiarasu, O.C. Zienkiewicz, Porous medium - fluid interface problems. The finite element analysis by using the CBS procedure, Int. J. Numer. Methods Heat Fluid Flow 11 (2001) 473–490.
[14] F. Arpino, A. Carotenuto, N. Massarotti, P. Nithiarasu, A robust model and numerical approach for solving solid oxide fuel cell (SOFC) problems, Int. J. Numer. Methods Heat Fluid Flow 18 (7–8) (2008) 811–834.
[15] F. Arpino, A. Carotenuto, N. Massarotti, A. Mauro, New solutions for axial flow convection in porous and partly porous cylindrical domains, Int. J. Heat Mass Transfer 57 (1) (2013) 155–170.
[16] S. Ergun, Fluid flow through packed column, Chem. Eng. Prog. 48 (1952) 89–94.
[17] S.K. Sinha, T. Sundararajan, V.K. Garg, A variable property analysis of alloy solidification using the anisotropic porous medium approach, Int. J. Heat Mass Transfer 35 (1992) 2865–2877.
[18] P. Nithiarasu, An efficient artificial compressibility (AC) scheme based on the characteristic based split (CBS) method for incompressible flows, Int. J. Numer. Methods Eng. 56 (2003) 1815–1845.
[19] F. Arpino, N. Massarotti, A. Mauro, P. Nithiarasu, Artificial compressibility-based CBS scheme for the solution of the generalized porous medium model, Numer. Heat Transfer B—Fundam. 55 (3) (2009) 196–218.
[20] P. Nithiarasu, K. Ravindran, A new semi-implicit time stepping procedure for buoyancy driven flow in a fluid saturated porous medium, Comput. Methods Appl. Mech. Eng. 165 (1998) 147–154.
[21] P. Nithiarasu, K.N. Seetharamu, T. Sundararajan, Double-diffusive natural convection in an enclosure filled with fluid-saturated porous medium: A generalized non-Darcy approach, Numer. Heat Transfer A—Appl. 30 (1996) 413–426.
[22] P. Nithiarasu, A comparative study on the performance of two time stepping schemes for convection in a fluid saturated porous medium, Int. J. Numer. Methods Heat Fluid Flow 11 (2001) 308–328.

[23] R.F. Berenati, C.B. Brosilow, Void fraction distribution in packed beds, AIChE J. 8 (1962) 359–361.
[24] K. Vafai, R.L. Alkire, C.L. Tien, An experimental investigation of heat transfer in variable porosity media, ASME J. Heat Transfer 107 (1984) 642–647.
[25] H.C. Brinkman, A calculation of viscous force exerted by a flowing fluid on a dense swarm of particles, Appl. Sci. Res. 1 (1947) 27–34.
[26] P. Forchheimer, Wasserbewegung durch bodem, Z. Ver. Deutsch. Ing. 45 (1901) 1782.
[27] H. Inaba, N. Seki, An experimental study of transient heat transfer characteristics in a porous layer enclosed between two opposing vertical surfaces with different temperatures, Int. J. Heat Mass Transfer 24 (1981) 1854–1857.
[28] E. David, G. Lauriat, P. Cheng, A numerical solution of variable porosity effects on natural convection in a packed sphere cavity, ASME J. Heat Transfer 113 (1991) 391–399.
[29] K.L. Walker, G.M. Homsy, Convection in a porous cavity, J. Fluid Mech. 87 (1978) 449–474.
[30] G. Lauriat, V. Prasad, Non-Darcian effects on natural convection in a vertical porous enclosure, Int. J. Heat Mass Transfer 32 (1989) 2135–2148.
[31] O.V. Trevisan, A. Bejan, Natural convection with combined heat and mass transfer buoyancy effects in porous medium, Int. J. Heat Mass Transfer 28 (1985) 1597–1611.
[32] V. Prasad, F.A. Kulacki, M. Keyhani, Natural convection in porous media, J. Fluid Mech. 150 (1985) 80.